JACS
JOURNAL OF THE AMERICAN CHEMICAL SOCIETY

Subscriber access provided by American Chemical Society

Article

Azide-Inhibited Bacterial Heme Oxygenases Exhibit an *S* = 3/2 (d,d)(d)(d) Spin State: Mechanistic Implications for Heme Oxidation

Yuhong Zeng, Gregori A. Caignan, Richard A. Bunce, Juan Carlos Rodrguez, Angela Wilks, and Mario Rivera

J. Am. Chem. Soc., **2005**, 127 (27), 9794-9807• DOI: 10.1021/ja0425987 • Publication Date (Web): 16 June 2005

Downloaded from http://pubs.acs.org on March 25, 2009

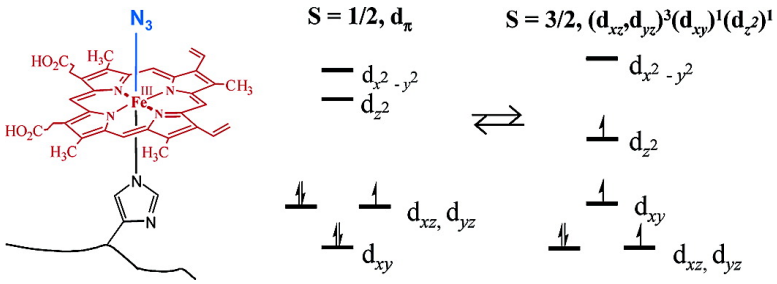

More About This Article

Additional resources and features associated with this article are available within the HTML version:

- Supporting Information
- Links to the 3 articles that cite this article, as of the time of this article download
- Access to high resolution figures
- Links to articles and content related to this article
- Copyright permission to reproduce figures and/or text from this article

View the Full Text HTML

ACS Publications
High quality. High impact.

Journal of the American Chemical Society is published by the American Chemical Society. 1155 Sixteenth Street N.W., Washington, DC 20036

J|A|C|S
ARTICLES
Published on Web 06/16/2005

Azide-Inhibited Bacterial Heme Oxygenases Exhibit an $S = 3/2$ $(d_{xz},d_{yz})^3(d_{xy})^1(d_{z^2})^1$ Spin State: Mechanistic Implications for Heme Oxidation

Yuhong Zeng,[£] Gregori A. Caignan,[£,‡] Richard A. Bunce,[§] Juan Carlos Rodríguez,[£] Angela Wilks,[&] and Mario Rivera*[,£]

Contribution from the Department of Chemistry, The University of Kansas, 1251 Wescoe Hall Drive, Lawrence, Kansas 66045-7582, Department of Chemistry, Oklahoma State University, Stillwater, Oklahoma 74078-3071, and Department of Pharmaceutical Sciences, School of Pharmacy, University of Maryland, Baltimore, Maryland 21201-1180

Received December 9, 2004; E-mail: mrivera@ku.edu

Abstract: The azide complexes of heme oxygenase from *Pseudomonas aeruginosa* (*pa*-HO) and *Neisseriae meningitidis* (*nm*-HO) have been studied with the aid of ^{1}H and ^{13}C NMR spectroscopy. These complexes have been shown to exist as an equilibrium mixture of two populations, one exhibiting an $S = {}^1/_2$, $(d_{xy})^2(d_{xz}, d_{yz})^3$ electron configuration and planar heme and a second with a novel $S = {}^3/_2$, $(d_{xz}, d_{yz})^3(d_{xy})^1(d_{z^2})^1$ spin state and nonplanar heme. At physiologically relevant temperatures, the equilibrium shifts in the direction of the population exhibiting the latter electron configuration and nonplanar heme, whereas at temperatures approaching the freezing point of water, the equilibrium shifts in the direction of the population with the former electronic structure and planar heme. These findings indicate that the microenvironment of the distal pocket in heme oxygenase is unique among heme-containing proteins in that it lowers the σ-donating (field strength) ability of the distal ligand and, therefore, promotes the attainment of heme electronic structures thus far only observed in heme oxygenase. When the field strength of the distal ligand is slightly lower than that of azide, such as OH^- (*J. Am. Chem. Soc.* **2003**, *125*, 11842), the corresponding complex exists as a mixture of populations with nonplanar hemes and electronic structures that place significant spin density at the meso positions. The ease with which these unusual heme electronic structures are attained by heme oxygenase is likely related to activation of meso carbon reactivity which, in turn, facilitates hydroxylation of a meso carbon by the obligatory ferric hydroperoxide intermediate.

Introduction

The degradation of heme is catalyzed by the enzyme heme oxygenase (HO).[1] Two isoforms of heme oxygenase (HO-1 and HO-2) have been unambiguously identified in mammalian cells.[2] HO-1 is induced by a variety of stimuli, including heme, oxidizing agents, hormones, and heavy metals, whereas HO-2 is constitutively expressed at highest concentrations in the brain and testes.[3] The products of HO activity, iron, carbon monoxide (CO), and biliverdin, have important biological functions. The release of iron from heme is crucial for iron recycling because less than 4% of daily iron requirements are absorbed from dietary intake.[4] Biliverdin and bilirubin are powerful antioxidants,[2,5,6] and CO has been implicated as a neural messenger,[7] modulator of vascular tone,[8,9] and protective agent in hemorrhagic shock.[10] HO enzymes have also been identified in plants[11] and bacteria,[12,13] where they degrade heme in a manner similar to that described above for mammalian cells. One difference is that in plants and bacteria the reducing equivalents needed to carry out the catalytic cycle are not supplied by cytochrome P450 reductase, but more likely by a ferredoxin.[14−16] In plants, photosynthetic bacteria, nonphotosynthetic bacteria, and fungi, the function of HO appears to be the degradation of heme to biliverdin for its subsequent use in the synthesis of tetrapyrrole-containing chromophores, phytochromes, and bacteriophyto-

[£] The University of Kansas.
[§] Oklahoma State University.
[&] University of Maryland.
[‡] Current address: Laboratory of Molecular Biophysics, The Rockefeller University, New York, New York 10021.

(1) Tenhunen, R.; Marver, H. S.; Schmid, R. *J. Biol. Chem.* **1969**, *244*, 6388−6394.
(2) Maines, M. D. *Annu. Rev. Pharmacol. Toxicol.* **1997**, *37*, 517−554.
(3) Otterbein, L. E.; Choi, A. M. K. *Am. J. Physiol. Lung Cell Mol. Physiol.* **2000**, *279*, L1029−L1037.
(4) Uzel, C.; Conrad, M. E. *Semin. Hematol.* **1998**, *35*, 27−34.
(5) Stocker, R.; Yamamoto, Y.; McDonagh, A. F.; Glazer, A. N.; Ames, B. N. *Science* **1987**, *235*, 1043−1046.
(6) Marilena, G. *Biochem. Mol. Med.* **1997**, *61*, 136−142.
(7) Verma, A.; Hirsch, D. J.; Glatt, C. E.; Ronnett, G. V.; Snyder, S. H. *Science* **1993**, *259*, 381−384.
(8) Kaide, J.-I.; Zhang, F.; Wei, Y.; Jiang, H.; Yu, C.; Wang, W.; Balazy, M.; Abraham, N. G.; Nasjletti, A. *J. Clin. Invest.* **2001**, *107*, 1163−1171.
(9) Zhang, F.; Kaide, J.-I.; Rodriguez-Mulero, F.; Abraham, N. G.; Nasjletti, A. *Am. J. Hypertens.* **2001**, *14*, 62S−67S.
(10) Pannen, B. H. J.; Köhler, N.; Hole, B.; Bauer, M.; Clemens, M. G.; Geiger, K. K. *J. Clin. Invest.* **1998**, *102*, 1220−1228.
(11) Muramoto, T.; Kohchi, T.; Yokota, A.; Hwang, I.; Goodman, H. M. *Plant Cell* **1999**, *11*, 335−347.
(12) Cornejo, J.; Beale, S. I. *Photosynth. Res.* **1997**, *51*, 223−230.
(13) Frankenberg-Dinkel, N. *Antioxid. Redox Signaling* **2004**, *6*, 825−834.
(14) Beale, S. I.; Cornejo, J. *Arch. Biochem. Biophys.* **1983**, *227*, 279−286.
(15) Beale, S. I. *Chem. Rev.* **1993**, *93*, 785−802.
(16) Wegele, R.; Tasler, R.; Zeng, Y.; Rivera, M.; Frankenberg-Dinkel, N. *J. Biol. Chem.* **2004**, *279*, 45791−45802.

10.1021/ja0425987 CCC: $30.25 **© 2005 American Chemical Society**

Scheme 1

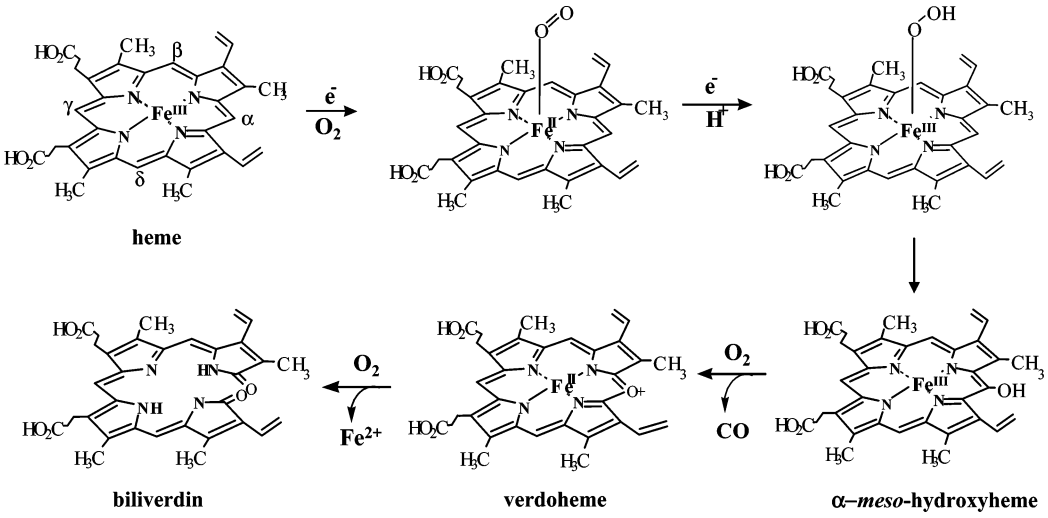

chromes, which are involved in light-sensing processes.[17,18] HO in pathogenic bacteria[19−22] is thought to play an important role in the release of iron from exogenously acquired heme for subsequent utilization in bacterial growth and host colonization (infection).

The first step in the catalytic cycle of heme degradation (see Scheme 1)[23] involves reduction of the ferric, resting state enzyme, to its ferrous form. This is followed by the coordination of molecular oxygen to yield an oxyferrous complex, which accepts a second electron and a proton to form a ferric hydroperoxide intermediate. The ferric hydroperoxide species hydroxylates the heme, typically at the α-meso carbon, producing α-mesohydroxyheme; the latter decays into verdoheme and CO in an oxygen-dependent manner, which is followed by the oxidation of verdoheme to iron−biliverdin in a process that also requires electrons and dioxygen.

Results obtained from investigating the reaction between HO and small amounts of H_2O_2 have been interpreted to indicate that the ferric hydroperoxide intermediate (Fe^{III}−OOH) in Scheme 1 is the oxidizing species that hydroxylates the heme in HO.[24] Spectroscopic support for this notion was obtained by radiolytic cryoreduction (77 K) of the oxyferrous complex of HO, which results in the formation of the EPR-active Fe^{III}−OOH intermediate.[25,26] Upon increasing the temperature to 218 K (annealing) for a short period and cooling back to 77 K, the EPR signal corresponding to the Fe^{III}−OOH intermediate is replaced by a signal corresponding to α-hydroxyheme.[25,26] Peroxidase and monooxygenase enzymes also form an Fe^{III}−OOH intermediate. However, the Fe^{III}−OOH intermediate in these enzymes rapidly decays into compound I or an oxoferryl species, which is responsible for the oxidative chemistry characteristic of these enzymes.[27] Hence, once formed, the Fe^{III}−OOH intermediate can follow at least two competing paths: the formation of an oxoferryl or the oxidation of heme to α-mesohydroxyheme. The reasons behind the distinct fate of the obligatory Fe^{III}−OOH intermediate, which in HO leads to heme hydroxylation and in peroxidase and monooxygenase enzymes to the formation of an Fe^{V}=O species, are not yet completely understood.

Studies performed with meso-^{13}C-labeled Fe^{III}−tetraphenylporphyrinates coordinated by a methoxide and alkyl hydroperoxide ligands, [meso-^{13}C-TPPFe(OCH$_3$)(OO^{t}Bu)]$^-$,[28] revealed the presence of an equilibrium (eq 1) between a planar heme with an $S = {}^1/_2$, $(d_{xy})^2(d_{xz}, d_{yz})^3$ electronic configuration (d_π hereafter) and a ruffled heme with the less common $S = {}^1/_2$, $(d_{xz},d_{yz})^4(d_{xy})^1$ electronic configuration ($(d_{xy})^1$ hereafter). At low temperatures, the equilibrium shifts to the left

$$\text{planar } (d_\pi) \overset{K_{eq}}{\rightleftharpoons} \text{ruffled } (d_{xy}) \qquad (1)$$

with almost 100% population of the planar d_π heme at 4 K, whereas at more elevated temperatures, the equilibrium shifts to the right, and at ambient temperatures, the fraction with the ruffled macrocycle and $(d_{xy})^1$ electronic configuration is expected to approach unity.[28] Ferrihemes with the $(d_{xy})^1$ electronic structure not only are ruffled but also are known to place relatively large amounts of spin density at the meso positions[29,30] and acquire significant a_{2u}-type cation radical character,[31] a property that makes them chemically noninnocent. It was, therefore, suggested that if a similar equilibrium between planar and ruffled hemes takes place within the confines of the heme pocket in HO, the relatively large electron density at the meso carbons would facilitate attack of the terminal OH group in the Fe^{III}−OOH complex.[28]

(17) Bhoo, S.-H.; Davis, S. J.; Walker, J.; Karniol, B.; Viestra, R. D. *Nature* **2001**, *414*, 776−779.
(18) Gambetta, G. A.; Lagarias, J. C. *Proc. Natl. Acad. Sci. U.S.A.* **2001**, *98*, 10566−10571.
(19) Wilks, A.; Schmitt, M. P. *J. Biol. Chem.* **1998**, *273*, 837−841.
(20) Schmitt, M. P. *J. Bacteriol.* **1997**, *179*, 838−845.
(21) Zhu, W.; Hunt, D. J.; Richardson, A. R.; Stojiljkovic, I. *J. Bacteriol.* **2000**, *182*, 439−447.
(22) Ratliff, M.; Zhu, W.; Deshmukh, R.; Wilks, A.; Stojiljkovic, I. *J. Bacteriol.* **2001**, *183*, 6394−6403.
(23) Ortiz de Montellano, P. R.; Auclair, K. In *The Porphyrin Handbook*; Guilard, R., Ed.; Elsevier: Amsterdam, 2003; Vol. 12, pp 183−210.
(24) Wilks, A.; Ortiz de Montellano, P. R. *J. Biol. Chem.* **1993**, *268*, 22357−22362.
(25) Davydov, R. M.; Yoshida, T.; Ikeda-Saito, M.; Hoffman, B. M. *J. Am. Chem. Soc.* **1999**, *121*, 10656−10657.
(26) Davydov, R.; Kofman, V.; Fujii, H.; Yoshida, T.; Ikeda-Saito, M.; Hoffman, B. M. *J. Am. Chem. Soc.* **2002**, *124*, 1798−1808.
(27) Colas, C.; Ortiz de Montellano, P. R. *Chem. Rev.* **2003**, *103*, 2305−2332.
(28) Rivera, M.; Caignan, G. A.; Astashkin, A. V.; Raitsimring, A. M.; Shokhireva, T. K.; Walker, F. A. *J. Am. Chem. Soc.* **2002**, *124*, 6077−6089.
(29) Safo, M. K.; Gupta, G. P.; Watson, C. T.; Simonis, U.; Walker, F. A.; Scheidt, W. R. *J. Am. Chem.* Soc. **1992**, *114*, 7066−7075.
(30) Walker, F. A. In *The Porphyrin Handbook*; Guilard, R., Ed.; Academic Press: New York, 2000; Vol. 5, pp 81−183.
(31) Ghosh, A.; Gonzalez, E.; Vangberg, T. *J. Phys. Chem. B* **1999**, *103*, 1363−1367.

These findings led the authors to propose that significant insights may be obtained from studying the electronic structure of the $Fe^{III}-OOH$ intermediate in HO catalysis at ambient temperatures. An obvious difficulty with this approach is the very high reactivity of this intermediate. In an attempt to circumvent this difficulty, the hydroxide complex of heme oxygenase from *Pseudomonas aeruginosa* (*pa*-HO) was used as a model of the corresponding hydroperoxide complex.[32] These investigations revealed that the hydroxide complex of *pa*-HO (*pa*-HO−OH) exists in the form of at least three populations of molecules in dynamic exchange, each exhibiting a distinct electronic configuration of the heme and nonplanar conformation.[32] The most abundant population was attributed to an $S = {}^1/_2$, $S = {}^3/_2$ spin state crossover species that is characterized by pyrrole carbon-α and carbon-β (C_α and C_β, respectively) resonances near 400 ppm and meso carbon (C_m) resonances near 40 ppm.[33] Two other populations were observed, one with a pure $S = {}^3/_2$, $(d_{xy})^2(d_{xz},d_{yz})^2(d_z{}^2)^1$ ($S = {}^3/_2$, d_π hereafter) electron configuration exhibiting C_α resonances at ca. 650 ppm, C_β resonances at ca. 1000 ppm, and C_m resonances at ca. −200 ppm, and the other with an $S = {}^1/_2$, $(d_{xy})^1$ electron configuration with corresponding C_m resonances near 1300 ppm and C_α resonances at ca. −400 ppm.[32] These electronic configurations are unusual among model hemes and highly unusual among heme active sites. More important, however, is the fact that ferric porphyrinates exhibiting the $(d_{xy})^1$ and $S = {}^3/_2$, d_π configurations are always associated with significant nonplanar distortions of the macrocycle,[33−38] and as indicated by the C_m chemical shifts, they can place significant spin density at the meso carbons.[32] In comparison, it is noteworthy that the hydroxide complexes of globins exhibit the more common d_π electron configuration typical of planar hemes.[39]

The unusual electronic structures observed with *pa*-HO−OH were attributed to a lowering of the hydroxide σ-bonding strength by virtue of accepting a hydrogen bond from a water molecule or amino acid in the distal pocket.[32] A decreased axial ligand field strength is typically accompanied by a shortening of the $Fe-N_{pyr}$ bonds (strengthening of the equatorial field) and stabilization of the $d_z{}^2$ orbital, which facilitates attainment of the $S = {}^3/_2$ electron configuration,[40,41] and/or stabilization of the d_{xz} and d_{yz} orbitals relative to the in-plane d_{xy} orbital, which is conducive to the $(d_{xy})^1$ electronic configuration.[29,38,42] In this report, we document efforts aimed at further probing the notion that modulation of the distal ligand field strength in HO enzymes promotes nonplanar distortions of the heme macrocycle and stabilization of unusual electronic structures that may be linked to heme hydroxylation reactivity. Azide was chosen as a distal ligand because it is capable of accepting a hydrogen bond by the coordinating N atom and typically exhibits a field strength that is only slightly stronger than that of the hydroxide ligand.[43] Two bacterial heme oxygenases, one from *Neisseriae meningitidis* (*nm*-HO) and a second from *Pseudomonas aeruginosa* (*pa*-HO), were studied to ensure that these observations are made in more than one HO enzyme. As will be shown below, the coordination of azide to the heme iron in HO induces a novel heme electronic structure that is associated with nonplanar heme distortions. The implications of these findings to the mechanism of heme hydroxylation are discussed in the context of this and previous investigations.

Experimental Section

Protein Preparation and Reconstitution with ^{13}C-Labeled Heme. Heme oxygenases from *Pseudomonas aeruginosa* (*pa*-HO) and from *Neisseriae meningitidis* (*nm*-HO) were expressed and purified as described previously.[22,44,45] ^{13}C-Labeled δ-aminolevulinic acid (ALA) was used as the biosynthetic precursor for the preparation of ^{13}C-labeled protoheme IX (heme) according to previously described methodology.[46,47] [5-^{13}C]-ALA, [4-^{13}C]-ALA, [3-^{13}C]-ALA, and [1,2-^{13}C]-ALA were synthesized according to methodology described previously.[48] [1,2-^{13}C]-ALA was used to prepare heme labeled at the methyl, propionate-β, and vinyl-β carbons. [5-^{13}C]-ALA was used to prepare heme labeled at the meso (C_m) and α-pyrrole (C_α) carbons; [4-^{13}C]-ALA was utilized to prepare heme labeled at the C_α and β-pyrrole (C_β) carbons, and [3-^{13}C]-ALA was used as a precursor of heme labeled at the C_β, α-vinyl, and α-propionate carbons. Isotopically labeled heme was purified in its complex with rat liver outer mitochondrial membrane (OM) cytochrome b_5,[46,47] and ^{13}C-labeled heme was then extracted from OM cytochrome b_5 by addition of 15 mL of pyridine to 2.5 mL of rat OM cytochrome b_5 (1 mM) in phosphate buffer ($\mu = 0.1$, pH = 7.0), followed by slow addition of chloroform (10−15 mL). This procedure typically results in precipitation of the polypeptide, while maintaining the pyridine hemochrome in the supernatant. The latter is separated from the precipitate by centrifugation and then dried over anhydrous $MgSO_4$. The desiccant is separated by filtration and the solution evaporated to dryness with the aid of a rotary evaporator. The solid is redissolved in 1−2 mL of dimethyl sulfoxide, and the resultant solution is immediately used to reconstitute HO. To this end, a solution (40 mL) containing approximately 2 μmol of *pa*-HO is titrated with the solution containing ^{13}C-labeled heme until the ratio of A_{280}/A_{Soret} no longer changes. The resulting solution is incubated at 4 °C overnight and subsequently purified on a Sephadex G-50 column (2.6 cm i.d. × 100 cm), previously equilibrated with phosphate buffer, $\mu = 0.1$ and pH = 7.0.

Spectroscopic Studies. NMR samples (300 μL, pH 7.0 phosphate buffer, and $\mu = 0.1$) were prepared in centrifugal concentrators equipped with 10 000 Da molecular weight cutoff membranes (Centricon-Millipore Co, Bedford, MA) and then transferred to Shigemi NMR tubes (5 mm) with susceptibilities matched to D_2O (Shigemi, Inc., Allison Park, PA). ^{1}H and ^{13}C NMR spectra were acquired on a Varian Unity Inova spectrometer operating at frequencies of 598.611 and 150.532 MHz, respectively. ^{1}H spectra were referenced to the residual water peak at 4.8 ppm, and ^{13}C spectra were referenced to an external solution

(32) Caignan, G. A.; Deshmukh, R.; Zeng, Y.; Wilks, A.; Bunce, R. A.; Rivera, M. *J. Am. Chem. Soc.* **2003**, *125*, 11842−11852.
(33) Ikeue, T.; Ohgo, Y.; Yamaguchi, T.; Takahashi, M.; Takeda, M.; Nakamura, M. *Angew. Chem., Int. Ed.* **2001**, *40*, 2617−2620.
(34) Safo, M. K.; Walker, F. A.; Raitsimring, A. M.; Walters, W. P.; Dolata, D. P.; Debrunner, P. G.; Scheidt, W. R. *J. Am. Chem. Soc.* **1994**, *116*, 7760−7770.
(35) Walker, F. A. *Coord. Chem. Rev.* **1999**, *186*, 471−534.
(36) Ikeue, T.; Saitoh, T.; Yamaguchi, T.; Ohgo, Y.; Nakamura, M.; Takahashi, M.; Takeda, M. *Chem. Commun.* **2000**, 1989−1990.
(37) Sakai, T.; Ohgo, Y.; Ikeue, T.; Takahashi, M.; Takeda, M.; Nakamura, M. *J. Am. Chem. Soc.* **2003**, *125*, 13028−13029.
(38) Yatsunyk, L. A.; Walker, F. A. *Inorg. Chem.* **2004**, *43*, 757−777.
(39) La Mar, G. N.; Satterlee, J. D.; De Ropp, J. S. In *The Porphyrin Handbook*; Guilard, R., Ed.; Academic Press: New York, 2000; Vol. 5, pp 185−297.
(40) Simonato, J.-P.; Pécaut, J.; Le Pape, L.; Oddou, J.-L.; Jeandey, C.; Shang, M.; Scheidt, W. R.; Wojaczynski, J.; Wolowiec, S.; Latos-Grazynski, L.; Marchon, J.-C. *Inorg. Chem.* **2000**, *39*, 3978−3987.
(41) Cheng, R.-J.; Chen, P.-Y.; Gau, P.-R.; Chen, C.-C.; Peng, S.-M. *J. Am. Chem. Soc.* **1997**, *119*, 2563−2569.
(42) Simonneaux, G.; Hindré, F.; Le Plouzennec, M. *Inorg. Chem.* **1989**, *28*, 823−825.
(43) Evans, D. R.; Reed, C. A. *J. Am. Chem. Soc.* **2000**, *122*, 4660−4667.
(44) Caignan, G. A.; Deshmukh, R.; Wilks, A.; Zeng, Y.; Huang, H.; Moënne-Loccoz, P.; Bunce, R. A.; Eastman, M. A.; Rivera, M. *J. Am. Chem. Soc.* **2002**, *124*, 14879−14892.
(45) Schuller, D. J.; Zhu, W.; Stojiljkovic, I.; Wilks, A.; Poulos, T. L. *Biochemistry* **2001**, *40*, 11552−11558.
(46) Rivera, M.; Walker, F. A. *Anal. Biochem.* **1995**, *230*, 295−302.
(47) Rivera, M.; Qiu, F.; Bunce, R. A.; Stark, R. E. *J. Biol. Inorg. Chem.* **1999**, *4*, 87−98.
(48) Bunce, R. A.; Shilling, C. L.; Rivera, M. *J. Labelled Compd. Radiopharm.* **1997**, *39*, 669−675.

of dioxane (60% v/v in D_2O) at 66.66 ppm. ^1H NMR spectra from HO solutions (~1.0 mM) were obtained with presaturation of the residual water peak, with an acquisition time of 250 ms and a 25 ms relaxation delay, over a spectral width of 30 kHz (low-spin samples) and 115 kHz (high-spin samples). ^{13}C NMR spectra were typically collected from solutions containing approximately 2 mM HO with a spectral width of 60 kHz over 48K data points, acquisition time of 80 ms, no relaxation delay, and 250 000 scans. HMQC spectra were typically acquired with spectral widths of 30 kHz for ^1H and 60 kHz for ^{13}C and a 25 ms relaxation delay.[49] Data were collected as an array of 2K × 256 points with 256 scans per t_1 increment and processed by zero-filling twice in both dimensions, apodized with a 90°-shifted squared sine bell, and Fourier transformed. NOESY spectra were acquired with 30 kHz spectral width in both dimensions, 2K data points in t_2, 256 increments in t_1, a 25 ms relaxation delay, 30 ms mixing time, and 256 scans. The data were processed by zero-filling in both dimensions, apodized with a 90°-shifted squared sine bell, and Fourier transformed.

Magnetic Susceptibility Measurements. A modification[50] of the Evans method[51] was used to measure magnetic susceptibilities. In short, a solution of the paramagnetic protein (*pa*-HO−N_3) was placed in the internal compartment of a coaxial NMR tube, and a solution of the diamagnetic form, in this case apo-*pa*-HO, was placed in the external compartment of the same coaxial tube. Protein concentration and solution conditions (phosphate buffer, pH 7.0, μ = 0.1, 10% D_2O, except for *pa*-HO−OH, which was prepared in 25 mM borate buffer at pH 10.0) were the same in both compartments of the coaxial tube; the solutions in each of the compartments contained 10 mM 1,4-dioxane as internal reference. The ^1H chemical shifts originating from dioxane in each of the compartments were measured at two fields, 800 MHz (Bruker Avance) and 600 MHz (Varian Unity Inova). No appreciable difference in the results was observed at the two different magnetic fields. The paramagnetic contribution to the molar susceptibility of the solute (χ_M^{para}) is related to the bulk susceptibility shift ($\Delta\delta$) as indicated by eq 2,[50,52] where χ_M^{para} is expressed in $m^3\ mol^{-1}$, $\Delta\delta$ is expressed in ppm, and M, the concentration of protein in solution, is expressed in mol L^{-1}. The magnetic moment in solution (μ_{eff}) was calculated using eq 3,[50,52] where T is absolute temperature, k is the Boltzmann constant, N_A is Avogadro's number, and μ_o is the permeability of vacuum.

$$\Delta\delta = \frac{1000 M \chi_M^{para}}{3} \tag{2}$$

$$\mu_{eff}^{\ 2} = \frac{\chi_M^{para} 3kT}{N_A \mu_o} \tag{3}$$

The concentration of paramagnetic protein was determined by electronic absorption spectroscopy using ϵ_{405} = 129 $mM^{-1}\ cm^{-1}$ for *pa*-HO and 179 $mM^{-1}\ cm^{-1}$ for *nm*-HO. The concentration of diamagnetic protein (the corresponding apoprotein) was also measured by electronic absorption spectroscopy using ϵ_{280} = 15.5 $mM^{-1}\ cm^{-1}$ for apo-*pa*-HO and ϵ_{280} = 28.2 $mM^{-1}\ cm^{-1}$ for apo-*nm*-HO. The extinction coefficients of the apoproteins were measured using a previously reported protocol.[53]

Results and Discussion

Characterization of the Azide Complexes of *nm*-HO and *pa*-HO by Electronic Absorption and ^1H NMR Spectroscopy. The high-frequency portion of the ^1H NMR spectrum of resting state *nm*-HO (Figure 1a) displays the large isotropic shifts and broad signals characteristic of $S = {}^5/_2$ hemoproteins. Addition of 1 equiv of sodium azide results in a decrease in intensity of these signals with the concomitant appearance of a set of narrower signals between 11 and 20 ppm (Figure 1c). The coexistence of signals corresponding to high-spin (*nm*-HO−H_2O) and *nm*-HO−N_3 indicates that these two complexes are in slow exchange relative to the NMR time scale; complete conversion to the *nm*-HO−N_3 complex requires the addition of 25 equiv of N_3^- (Figure 1e). Similar observations were made upon addition of NaN_3 to the resting state of *pa*-HO, except that 15 equiv was needed for the quantitative formation of the *pa*-HO−N_3 complex (Figure S1e in Supporting Information). The visible portion of the electronic absorption spectra of the *nm*-HO−N_3 and *pa*-HO−N_3 complexes were obtained by transferring a portion of the solution contained in an NMR tube to a 0.10 cm path-length cuvette, before and after the addition of N_3^- or CN^- (Figure 2a,b, respectively). The electronic absorption spectrum of resting state *nm*-HO at pH 7.0 (Figure 2a, black) shows a band at 504 nm and the characteristic high-spin marker at 638 nm. Addition of 10 equiv of CN^- results in complete conversion to the *nm*-HO−CN complex, which displays the spectrum shown in red. This spectrum shows the complete disappearance of the high-spin marker band, as is expected for a low-spin complex. Addition of 25 equiv of N_3^- to the resting state enzyme results in complete conversion to the *nm*-HO−N_3 complex, which displays the ^1H NMR spectrum of Figure 1e and the electronic absorption spectrum shown in Figure 2a, blue. The visible portions of the spectra from *nm*-HO−N_3 and *nm*-HO−CN are clearly distinct, whereas the corresponding Soret bands (Figure 2c) are very similar. An interesting feature of the visible portion of the *nm*-HO−N_3

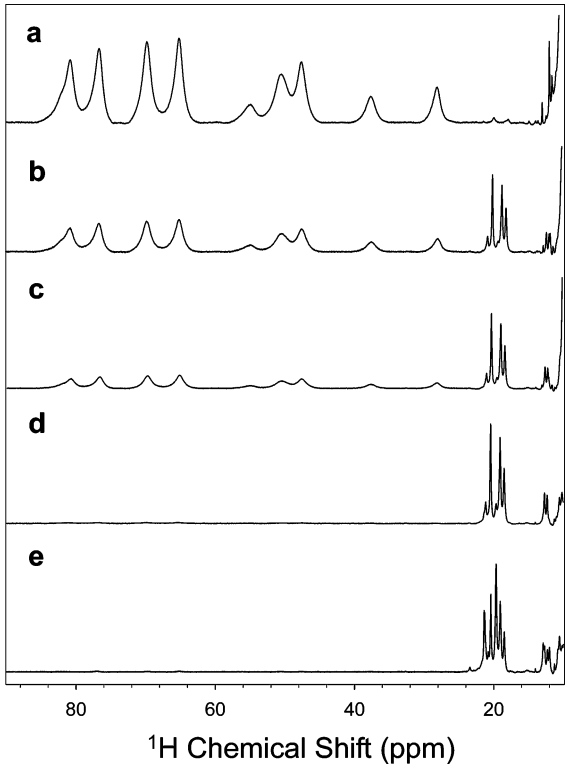

Figure 1. High-frequency portion of the ^1H NMR spectra of *nm*-HO obtained at 25 °C in the resting state (a), after addition of 0.5 (b), 1 (c), 15 (d), and 25 (e) equiv of sodium azide.

(49) Summers, M. F.; Marzilli, L. G.; Bax, A. *J. Am. Chem. Soc.* **1986**, *108*, 4285−4294.
(50) Bertini, I.; Luchinat, C.; Turano, P.; Battaini, G.; Casella, L. *Chem.—Eur. J.* **2003**, *9*, 2316−2322.
(51) Evans, D. F. *J. Chem. Soc.* **1959**, 2003−2005.
(52) Bertini, I.; Luchinat, C. *Coord. Chem. Rev.* **1996**, *150*, 1−296.
(53) Gill, S. C.; von Hippel, P. H. *Anal. Biochem.* **1989**, *182*, 319−326.

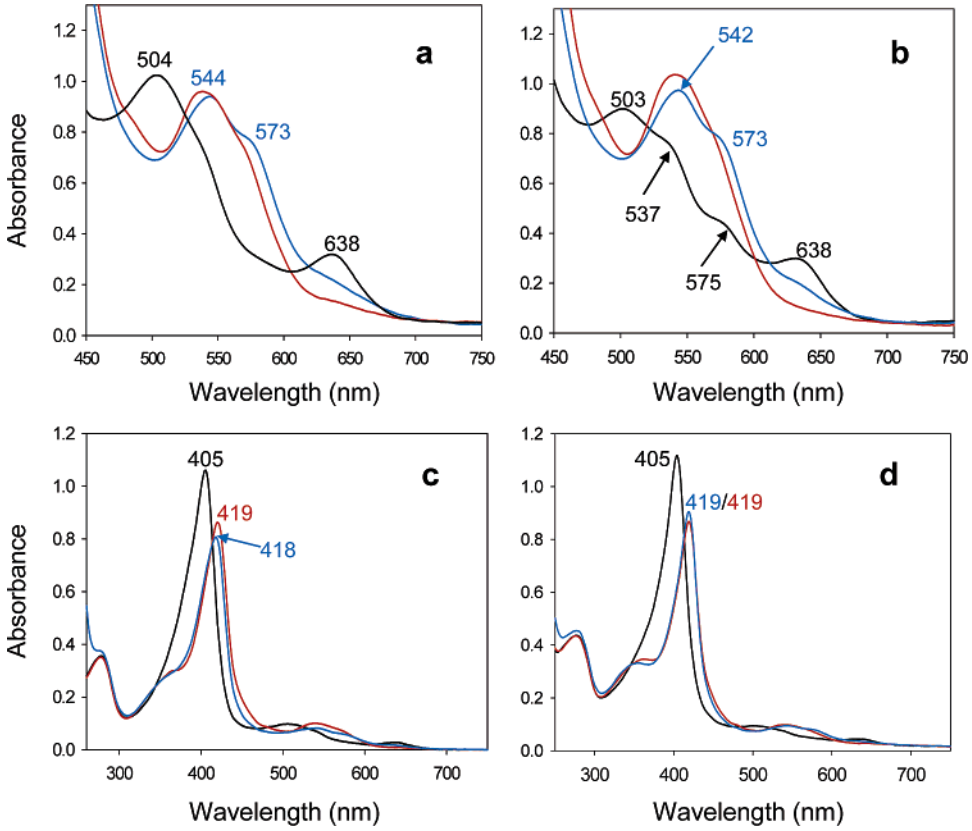

Figure 2. Electronic absorption spectra showing the (a) visible and (c) Soret bands of *nm*-HO−H_2O (black), *nm*-HO−CN obtained after the addition of 10 equiv of NaCN (red), and *nm*-HO−N_3 obtained after addition of 25 equiv of NaN_3 (blue). (b) and (d) Display of the visible and Soret bands of *pa*-HO−H_2O (black), *pa*-HO−CN obtained upon addition of 10 equiv of NaCN (red) and *pa*-HO−N_3 obtained upon addition of 15 equiv of NaN_3 (blue). Spectra in (a) and (b) were obtained in a 0.1 cm cuvette with protein concentrations of ~1.0 mM, and spectra in (c) and (d) were obtained in a 1 cm cuvette with protein concentrations of ~10 μM.

spectrum is the presence of a small band near 635 nm, which is reminiscent of the high-spin marker band at 638 nm. While this band can be taken to suggest that there is a significant contribution from resting state (high-spin) species to the spectrum, this idea is not consistent with (i) the complete disappearance of resonances corresponding to a high-spin complex in the ^{1}H NMR spectrum obtained after addition of 25 equiv of N_3^- (Figure 1e) and (ii) the features of the visible (Figure 2a) and Soret (Figure 2c) regions of the UV−vis spectrum, which are very different from those exhibited by the high-spin aqua complex. Hence, the ^{1}H NMR and electronic absorption spectra shown in Figures 1e and 2a,c are consistent with complete conversion of the high-spin *nm*-HO aqua complex into the corresponding azide complex. However, differences between the electronic absorption spectra of *nm*-HO−N_3 and *nm*-HO−CN, which are more noticeable in the visible region (Figure 2a), suggest that *nm*-HO−N_3 does not have a pure d_π spin state. Similar observations were made with *pa*-HO. The spectrum of resting state *pa*-HO at pH 7.0 (black in Figure 2b) exhibits a band at 503 nm and a high-spin marker band at 638 nm, thus indicating that the enzyme is in the high-spin state. The shoulders at 537 and 575 nm, however, are indicative of the presence of a low-spin component. The low-spin bands originate from the ferric−hydroxide complex (*pa*-HO−OH), which is in equilibrium with the resting state aqua complex; the ferric−aqua to ferric−hydroxide equilibrium in *pa*-HO has been reported to occur with a $pK_a \sim 8.1$.[32] Addition of 15 equiv of N_3^- to resting state *pa*-HO results in complete conversion to the *pa*-HO−N_3 complex, which displays the electronic absorption spectrum shown by the blue trace in Figure 2b, whereas addition of 10 equiv of CN^- results in the spectrum shown by a red trace in the same figure. Again, the most significant differences between the *pa*-HO−CN and *pa*-HO−N_3 spectra also occur in the visible region (Figure 2b), where the presence of a weak band near 635 nm in the spectrum of *pa*-HO−N_3 (Figure 2b, blue) stands in contrast to the complete disappearance of a similar band in the *pa*-HO−CN complex (red). As indicated above, this band in the spectrum of *pa*-HO−N_3 does not arise from high-spin *pa*-HO because the visible bands and the Soret band (Figure 2b,d, blue) in the electronic absorption spectrum and the corresponding ^{1}H NMR spectrum (Figure S1e) indicate complete disappearance of the high-spin species. It will be shown below that the unique features of the visible portions of the electronic absorption spectra of *pa*-HO−N_3 and *nm*-HO−N_3 are likely a manifestation of species with an intermediate spin state ($S = {}^3/_2$).

The ^{1}H NMR spectra of the *nm*-HO−N_3 and *pa*-HO−N_3 complexes are shown in Figure 3B,D, respectively. The high-frequency portions of these spectra are significantly different from the corresponding regions in the spectra of the well characterized *nm*-HO−CN and *pa*-HO−CN complexes.[44,54] The spectrum of *nm*-HO−CN (Figure 3A) is typical of α-hydroxylating HO enzymes in that only the 3Me resonance is resolved above 12 ppm,[16,32,55] whereas the spectrum of the *pa*-HO−CN

(54) Liu, Y.; Zhang, X.; Yoshida, T.; La Mar, G. N. *Biochemistry* **2004**, *43*, 10112−10126.
(55) Zeng, Y.; Deshmukh, R.; Caignan, G. A.; Bunce, R. A.; Rivera, M.; Wilks, A. *Biochemistry* **2004**, *43*, 5222−5238.

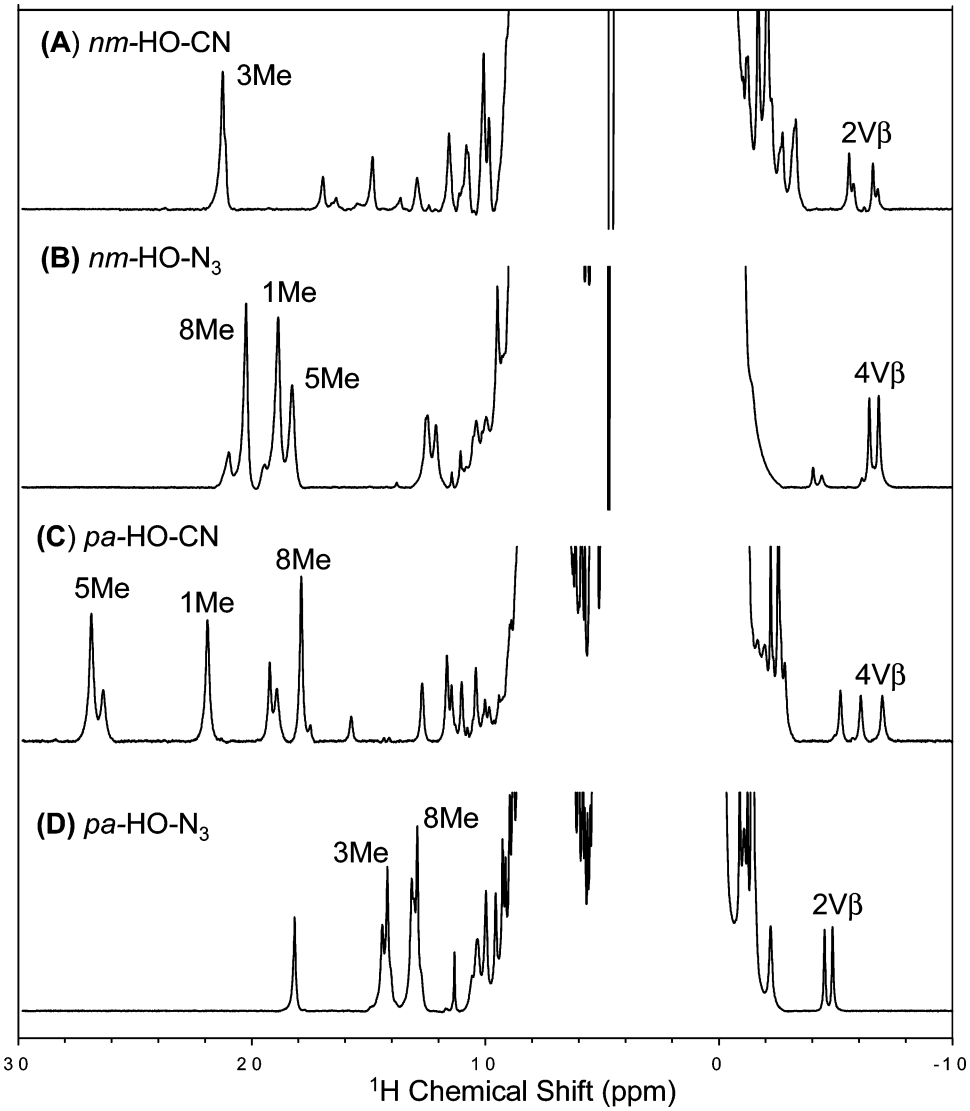

Figure 3. ^{1}H NMR spectra of cyanide- and azide-inhibited HO complexes acquired at 25 °C.

complex (Figure 3C), which shows three heme methyl resonances (5Me, 1Me, and 8Me), has only been observed with this enzyme because its heme is rotated in-plane by approximately 100° relative to the heme in α-hydroxylating enzymes.[44,56] The pronounced differences in the patterns of heme methyl shifts between the cyano and azido complexes of *nm*-HO and *pa*-HO can, in principle, be attributed to in-plane heme rotation or a change in conformation of the proximal ligand upon binding of the N_3^- ligand. Experimental observations discussed in the following section, however, indicate that this is unlikely. In addition, the structure of the azide complex of rat HO-1 has been determined and shown to have a structure almost identical to that of the resting state enzyme.[57] Instead, the patterns of heme methyl resonances exhibited by the *nm*-HO−N_3 and *pa*-HO−N_3 complexes are reminiscent of the pattern exhibited by the most abundant population of *pa*-HO−OH, which was shown to exist as a mixture of at least three populations with unusual electronic configurations and nonplanar heme distortions.[32] It will be shown below that the differences in the ^{1}H NMR spectra of CN^- and N_3^- complexes of *nm*-HO and *pa*-HO are a consequence of these complexes acquiring different electronic structures.

Heme Methyl ^{1}H Chemical Shifts Indicate that the Electronic Configuration of the Heme in the *nm*-HO−N_3 and *pa*-HO−N_3 Complexes is not d_π. ^{1}H and ^{13}C NMR resonance assignments of heme substituents were carried out with the aid of one- and two-dimensional homo- and heteronuclear experiments. Heme labeled with ^{13}C at appropriate positions was used to reconstitute samples of *nm*-HO and *pa*-HO, followed by the formation of the corresponding azide complexes by addition of 25 and 15 equiv of NaN_3, respectively. The strategy followed to obtain the assignments has been previously documented in detail[16,44,55,58] and relies on the identification of ^{1}H and ^{13}C resonances utilizing enzyme reconstituted with ^{13}C-labeled heme. The ^{1}H resonance assignments (Table 1) are subsequently obtained with the aid of WEFT-NOESY experiments (Figure 4 and Figure S2).

The magnitude and spread of heme methyl ^{1}H chemical shifts originating from ferrihemes with the d_π electronic structure have been semiquantitatively correlated to the orientation of the

(56) Friedman, J.; Lad, L.; Li, H.; Wilks, A.; Poulos, T. L. *Biochemistry* **2004**, *43*, 5239−5245.
(57) Sugishima, M.; Sakamoto, H.; Higashimoto, Y.; Omata, Y.; Hayashi, S.; Noguchi, M.; Fukuyama, K. *J. Biol. Chem.* **2002**, *277*, 45086−45090.
(58) Rivera, M.; Caignan, G. A. *Anal. Bioanal. Chem.* **2004**, *378*, 1464−1483.

Table 1. ^{1}H and ^{13}C NMR Chemical Shifts for the *nm*-HO−N_3 and *pa*-HO−N_3 Complexes at 25 °C and pH 7.0

	nm-HO–N_3		*pa*-HO–N_3[a]	
position	^{1}H (ppm)	^{13}C (ppm)	^{1}H (ppm)	^{13}C (ppm)
1Me	18.90	−19.77	6.29	−1.12
3Me	8.17	3.90	14.15	−17.21
5Me	18.31	−16.91	5.96	−3.40
8Me	20.26	−22.70	12.91	−14.38
2-Vα	9.52	100.61	14.41	60.66
2-Vβ	0.53, 1.38	155.52	−4.89, −4.54	185.68
4-Vα	12.13	61.82	8.39	96.94
4-Vβ	−6.75, −6.35	194.31	0.08, 0.60	147.38
meso-α				
meso-β	1.57	12.43		
meso-γ	2.62	29.99		
meso-δ	3.09	35.49		
6-P-α	6.35, 10.07	9.26	5.36, 8.54	−9.34
6-P-β	0.89, 1.45	81.38	−1.12, −2.26	99.94
7-P-α	6.41, 10.43	7.82	8.63, 10.30	−14.63
7-P-β	0.51, 0.84	77.26	0.27, −0.04	104.86

[a] ^{1}H signals from meso groups in *pa*-HO appear to be broadened beyond detection.

proximal histidine−imidazole plane relative to the molecular *x*-axis, the angle ϕ in Figure 5.[59−62] When the distal ligand is axially symmetric (CN^- or N_3^-), this correlation is based mainly on interactions between the proximal histidine imidazole π orbitals, which lie perpendicular to the porphyrin plane, and the iron d_{xz} and d_{yz} (d_π) orbitals, which in turn interact individually with the porphyrin 3e(π) orbitals. Hence, these orbital interactions, which are affected by the angle that the proximal histidine−imidazole plane makes with the molecular *x*-axis (angle ϕ), lift the degeneracy of the porphyrin 3e(π) orbitals and determine the degree of uneven distribution of electron density among the porphyrin macrocycle.[61,62] An expression containing heuristically determined parameters (eq 4) has been derived for ferriheme centers coordinated by a proximal histidine and a distal, axially symmetric ligand.[63] In this expression, the angle ϕ is defined as above, θ_i is defined as the angle formed between the *i*th methyl−Fe axis and the molecular *x*-axis (see Figure 5), and δ_i is the calculated ^{1}H chemical shift of the corresponding heme methyl.

$$\delta_i = a \sin^2(\theta_i - \phi) + b \cos^2(\theta_i + \phi) + c \qquad (4)$$

The plot shown in Figure 5a was constructed with eq 4 utilizing heuristic values,[63] $a = 18.4$ ppm, $b = -0.8$ ppm, and $c = 6.1$ ppm, to facilitate visual correlations between calculated heme methyl ^{1}H shifts and the angle ϕ. The order and spread of experimental heme methyl ^{1}H chemical shifts obtained from the *nm*-HO−CN complex are 3Me > 8Me > 5Me > 1Me (Table 2) and correspond to an angle ϕ of ∼ 135° in the plot of Figure 5a; this value is in good agreement with that obtained from the crystal structure of *nm*-HO.[45] Similarly, the order and spread of experimental heme methyl ^{1}H shifts obtained from *pa*-HO−CN are 5Me > 1Me > 8Me > 3Me and corresponds to an angle ϕ of ∼33°, a value in good agreement with that found in the crystal structure of *pa*-HO.[56] In stark contrast, the order and spread of the experimental heme methyl shifts obtained from *nm*-HO−N_3 (8Me > 1Me > 5Me >3Me) and *pa*-HO−N_3 (3Me > 8Me > 1Me > 5Me) do not fit any angle ϕ in the plot of Figure 5a. These observations strongly argue against in-plane heme rotation upon binding of azide and suggest that the *nm*-HO−N_3 and *pa*-HO−N_3 complexes do not acquire the common d_π electronic configuration. This point is further illustrated in the following analysis: ^{1}H chemical shifts for each of the four methyl groups in *nm*-HO, *pa*-HO, and HO from *Corynebacterium diphtheriae* (*cd*-HO) were calculated with the aid of eq 4 and the angle ϕ observed in the corresponding crystal structures.[45,56,64] When the calculated values are plotted (Figure 5b) against the experimental values obtained from *nm*-HO−CN (pink circles), *pa*-HO−CN (blue circles), and *cd*-HO−CN (black circles), one obtains a good correlation, as is expected for a ferriheme center with a d_π electron configuration.[59,63] In contrast, when the calculated chemical shifts for *nm*-HO and *pa*-HO are plotted against the experimental ^{1}H shifts obtained from *nm*-HO−N_3 (red squares) and *pa*-HO−N_3 (green triangles), no correlation exists, indicating that the heme iron in the *nm*-HO−N_3 and *pa*-HO−N_3 complexes does not attain the d_π electron configuration.

Evans Measurements of Magnetic Susceptibility. The electronic absorption and ^{1}H NMR spectroscopic data discussed above suggest that the *nm*-HO−N_3 and *pa*-HO−N_3 complexes do not have a d_π electron configuration. The magnetic moment of these complexes was, therefore, measured in an attempt to ascertain the spin state of the HO−N_3 complexes. Hence, results from measuring the paramagnetic contribution to the molar susceptibility (χ_M^{para}) and subsequent calculation of the effective magnetic moment (μ_{eff}) of the paramagnetic center in the CN^- and N_3^- complexes of *pa*-HO and *nm*-HO, and in *nm*-HO−H_2O and *pa*-HO−OH complexes, are summarized in Table 3. Equation 2 indicates that the bulk susceptibility shift ($\Delta\delta$) is directly proportional to χ_M^{para}, and the data in Table 3 reveal that at any given temperature the values of $\Delta\delta$ and χ_M^{para} corresponding to the N_3^- complexes of *nm*-HO and *pa*-HO are approximately halfway between the values obtained for the corresponding CN^- ($S = {}^1/_2$) and aqua ($S = {}^5/_2$) complexes. The μ_{eff} values from the CN^- complexes of *nm*-HO and *pa*-HO and those corresponding to the resting state (aqua) of *nm*-HO are temperature independent (as expected), and their magnitudes are in good agreement with values corresponding to complexes with pure $S = {}^1/_2$ and $S = {}^5/_2$ spin states, respectively. In comparison, it is clear that the magnitudes of the μ_{eff} values obtained from *nm*-HO−N_3, *pa*-HO−OH, and *pa*-HO−N_3 do not correspond to complexes with $S = {}^1/_2$ or $S = {}^5/_2$ spin states. Moreover, these μ_{eff} values are temperature dependent, increasing approximately 0.1 for each 10 °C increment in temperature; this increase is significantly higher than the standard deviation obtained from triplicate measurements, which is ±0.01.

The magnitude and temperature dependence of μ_{eff} values obtained from *nm*-HO−N_3 and *pa*-HO−N_3 can be interpreted either as a mixture of $S = {}^1/_2$ and $S = {}^3/_2$ species or as a mixture of $S = {}^1/_2$ and $S = {}^5/_2$ species. Interpretation of the data in the context of a mixture of high-spin and low-spin species, however, is not consistent with several key observations. If equilibrium

(59) Shokhirev, N. V.; Walker, F. A. *J. Biol. Inorg. Chem.* **1998**, *3*, 581−594.
(60) Shokhirev, N. V.; Walker, F. A. *J. Am. Chem. Soc.* **1998**, *120*, 981−990.
(61) Walker, F. A. *J. Am. Chem. Soc.* **1980**, *102*, 3254−3256.
(62) Walker, F. A.; Buehler, J.; West, J. T.; Hinds, J. L. *J. Am. Chem. Soc.* **1983**, *105*, 6923−6929.
(63) Bertini, I.; Luchinat, C.; Parigi, G.; Walker, F. A. *J. Biol. Inorg. Chem.* **1999**, *4*, 515−519.
(64) Unno, M.; Matsui, T.; Chu, G. C.; Couture, M.; Yoshida, T.; Rousseau, D. L.; Olson, J. S.; Ikeda-Saito, M. *J. Biol. Chem.* **2004**, *279*, 21055−21061.

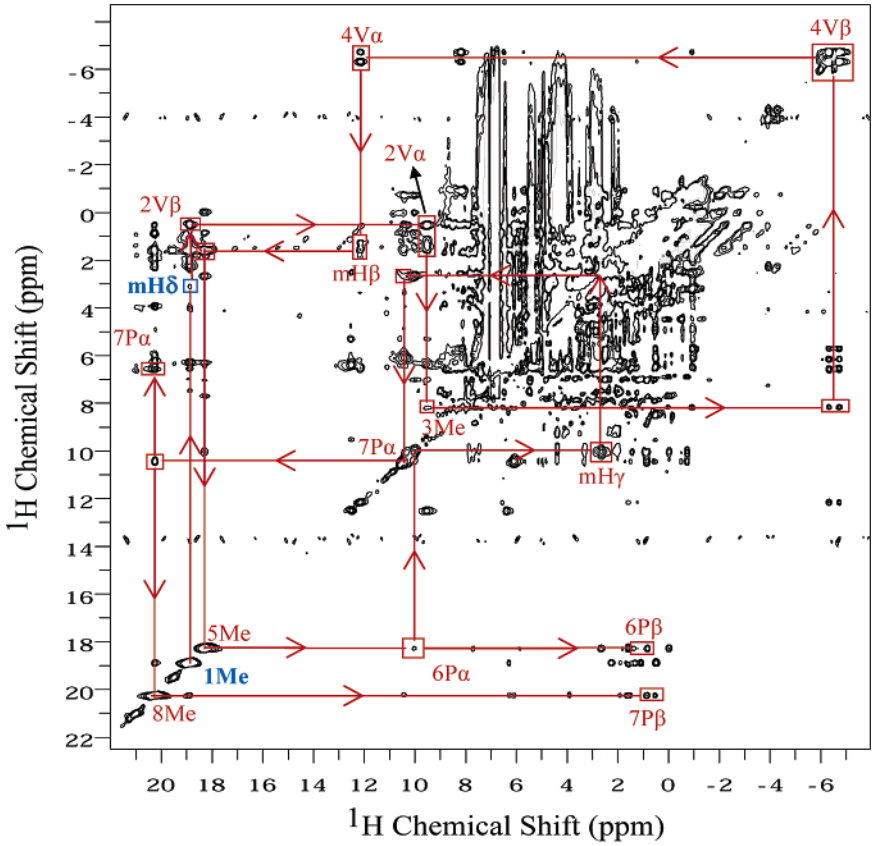

Figure 4. WEFT-NOESY spectrum of *nm*-HO−N_3 acquired at 25 °C. The arrows indicate dipolar connectivities that permit resonance assignments. These can be followed starting with meso-H_δ as a unique entry point,[55,58] which exhibits a dipolar connectivity to 1Me. The assignments can then be traced as follows: 1Me → $2V_\beta$ → $2V_\alpha$ → 3Me → $4V_\beta$ → $4V_\alpha$ → meso-H_β → 5Me → $6P_\alpha$→ meso-H_γ → $7P_\alpha$→ 8Me. Resonances corresponding to $6P_\beta$ and $7P_\beta$ can be identified by their respective cross-peaks with 5Me and 8Me.

between $S = {}^5/_2$ and $S = {}^1/_2$ species is assumed, the magnitude of the magnetic moment of HO−N_3 (Table 3) would indicate approximately 40% $S = {}^5/_2$ character. Such mixture should have a profound influence on the corresponding ^{1}H NMR spectrum. Hence, if the system is in slow exchange, as is the case for the HO−H_2O and HO−N_3 complexes, one should clearly observe the resonances originating from the ∼40% high-spin species. In fact, the NMR data (Figures 1, S1, and S3) demonstrate complete absence of high-spin resonances in *pa*-HO−N_3 and *nm*-HO−N_3 at 25 °C and only traces (<3%) of a high-spin component in *nm*-HO−N_3 at 35 °C upon addition of 25 (or 15) equiv of NaN_3 to resting state *nm*-HO (or *pa*-HO). Similarly, increasing the pH of the solution to 10 results in complete formation of the *pa*-HO−OH complex and complete disappearance of peaks corresponding to the high-spin resting state.[32] It is also interesting to consider that La Mar and co-workers have shown that the azide complex of sperm whale myoglobin (Mb-N_3) is in fast exchange between high-spin and low-spin species; at 25 °C, the fraction of high-spin character is ∼20%.[39,65] The heme methyl resonances from sperm whale met-Mb-N_3 are 5Me (31.6 ppm) > 1Me (26.2 ppm) > 8Me (24.4 ppm) > 3Me (9.3 ppm). In comparison, the heme methyl chemical shifts from sperm whale met-Mb-CN are[39] 5Me (27.0 ppm) > 1Me (18.6 ppm) > 8Me (12.9 ppm) > 3Me (4.8 ppm). Hence, fast exchange between $S = {}^5/_2$ and $S = {}^1/_2$ species in met-Mb-N_3 is manifested in downfield shifts for each of the four heme methyl resonances, relative to the corresponding resonances in met-Mb-CN (pure $S = {}^1/_2$). This downfield shift is expected because all heme methyl resonances in $S = {}^5/_2$ complexes are significantly downfield shifted; the average heme methyl chemical shift in met-Mb-H_2O is 76 ppm.[65] In this context, it is important to note that three of the heme methyl resonances in *pa*-HO−N_3 are significantly upfield shifted relative to those in *pa*-HO−CN, and one heme methyl resonance in *nm*-HO−N_3 is significantly upfield shifted relative to its counterpart in *nm*-HO−CN (Table 2). Thus, the HO−N_3 complexes are not in fast exchange between $S = {}^5/_2$ and $S = {}^1/_2$ species and behave differently from the Mb-HO−N_3 complexes.

Consequently, the magnitude and temperature dependence of μ_{eff} values obtained from *nm*-HO−N_3, *pa*-HO−N_3, and *pa*-HO−OH are consistent with a mixture of low-spin and intermediate spin ($S = {}^3/_2$) species. The magnitudes of μ_{eff} suggest that the $S = {}^3/_2$ spin state is more populated than the $S = {}^1/_2$ state at the higher temperatures studied; the data in Table 3 also suggest that lowering the temperature results in an increased population of the $S = {}^1/_2$ spin state. However, it is interesting to note that even at the low temperatures, the values of μ_{eff} suggest that the population with $S = {}^3/_2$ is still significant. In the following section, we describe how analysis of core heme carbon resonances corroborate this conclusion and permit elucidation of the electronic configuration in the $S = {}^3/_2$ spin state.

Probing the Electronic Structure of HO−N_3 Complexes with the Aid of Porphyrin Core Carbon Chemical Shifts. Recent studies conducted with ferrihemes have shown that chemical shifts originating from porphyrin core carbons, C_α, C_β, and C_m, constitute an excellent diagnostic tool to elucidate

(65) La Mar, G. N.; Budd, D. L.; Smith, K. M. *Biochim. Biophys. Acta* **1980**, *622*, 210−218.

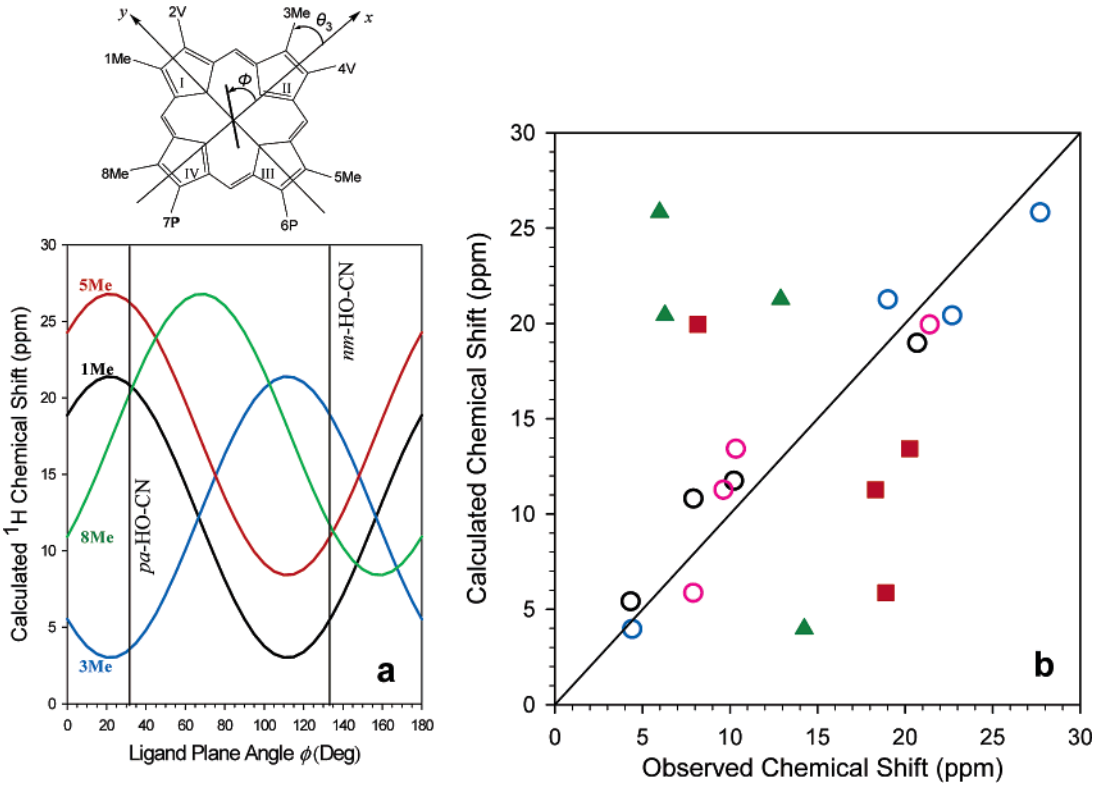

Figure 5. (Top left) Coordinate system and nomenclature used for describing the projection of the His−imidazole plane onto the porphyrin ring. The *x*-axis is aligned along the nitrogen atoms of pyrrole rings II and IV, the *y*-axis along the nitrogen atoms of pyrrole rings I and III, and the *z*-axis is normal to the heme. Plot (a) depicts the dependence of the calculated heme methyl ^{1}H shifts on ϕ, the angle between the molecular *x*-axis and the projection of the imidazole plane. The heme methyl ^{1}H chemical shifts were calculated with eq 4. Plot (b) correlates experimental methyl ^{1}H chemical shifts from different HO complexes with chemical shifts calculated with eq 4. Open circles correspond to the CN^- complexes of *nm*-HO (pink), *pa*-HO (blue), and *cd*-HO (black). Red squares correspond to *nm*-HO−N_3 and green triangles to *pa*-HO−N_3.

Table 2. Methyl ^{1}H Chemical Shifts of Cyano and Azido Complexes of *nm*-HO and *pa*-HO

position	*nm*-HO–CN[a]	*pa*-HO–CN[b]	*nm*-HO–N_3	*pa*-HO–N_3
1Me	7.90	22.69	18.90	6.29
3Me	21.40	4.41	8.17	14.15
5Me	9.62	27.71	18.31	5.96
8Me	10.33	19.01	20.26	12.91

[a] Obtained from ref 54, 25 °C. [b] Obtained from ref 44, 10 °C.

heme electronic structure.[32,33,36,58,66,67] For instance, symmetry allows overlap between porphyrin 3e(π) orbitals and iron d_π orbitals (d_{xz}, d_{yz}), and the relative sizes of the circles in the schematic representation of the 3e(π) orbitals (Figure 6) suggest that porphyrin-to-metal spin delocalization would induce significant spin density at the C_β carbons, smaller spin density at the C_α, and negligible spin density at the C_m positions. As a consequence, complexes with the d_π electronic structure exhibit downfield C_β chemical shifts, shown schematically in Figure 6a. Ferrihemes with the $S = {}^3/_2$, d_π electronic configuration have one unpaired electron in each of the d_π orbitals. Hence, porphyrin-to-metal spin delocalization can occur from the porphyrin 3e(π) orbitals into each of the two d_π orbitals, thus suggesting significantly larger spin density at the C_α and C_β positions. Indeed, ferrihemes with a pure $S = {}^3/_2$, d_π electronic configuration display very large downfield C_β shifts (~1000 ppm), large C_α shifts (~700 ppm), and by polarization, large and negative (upfield) C_m shifts (~−200 ppm)[32,33,58] (Figure 6b). Ferrihemes with the $S = {}^1/_2$, $(d_{xy})^1$ electronic structure are known to be ruffled;[34] the symmetry of hexacoordinated ferrihemes with a ruffled porphyrin (D_{2d}) allows overlap between the iron d_{xy} and porphyrin $a_{2u}(\pi)$ orbital because these orbitals have the same representation, b_2 (see Table 4). Thus, porphyrin-to-metal spin delocalization from the $a_{2u}(\pi)$ orbital to the iron d_{xy} orbital suggests large spin density at the meso carbons and, therefore, large downfield C_m shifts. In fact, ferrihemes with the $(d_{xy})^1$ electronic structure exhibit very large downfield C_m shifts (~1200 ppm) and, by polarization, large upfield (~−400 ppm) C_α shifts[32,67] (Figure 6c).

The ^{13}C NMR spectrum obtained from a solution of *nm*-HO−N_3 reconstituted with heme labeled at the C_β positions is shown in Figure 7a, and the spectrum of this complex reconstituted with heme labeled at the C_α and C_m positions is shown in Figure 7b. For comparison, the spectra corresponding to the cyano complexes labeled at equivalent positions are shown in Figure 7c,d, respectively. The *nm*-HO−CN complex possesses a pure d_π electronic structure and, therefore, exhibits average C_β shifts of 109 ppm and average C_α shifts of 25 ppm. These average values are in good agreement with average C_β shifts observed with ferrihemes possessing the d_π electronic structure.[47,58,66] In comparison, the average downfield C_β and C_α shifts obtained from the *nm*-HO−N_3 complex at the same temperature, 286 and 263 ppm, respectively (Figure 7a,b), are significantly larger.

The temperature dependence of heme core carbon shifts was studied between 2 and 35 °C. The plot in Figure 8a illustrates the behavior observed for C_α, C_β, and C_m shifts corresponding

(66) Mispelter, J.; Momenteau, M.; Lhoste, J. M. In *Biological Magnetic Resonance*; Reuben, J., Ed.; Plenum Press: New York, 1993; Vol. 12, pp 299−355.
(67) Ikeue, T.; Ohgo, Y.; Takashi, S.; Nakamura, M.; Fujii, H.; Yokoyama, M. *J. Am. Chem. Soc.* **2000**, *122*, 4068−4076.

Table 3. Magnetic Susceptibility Data for *Pa*-HO and *nm*-HO Complexes[a]

		CN^-			N_3^-			H_2O[d]			OH^- [e]		
protein	temp (K)	$\Delta\delta$ (Hz)	χ_M^{para}	μ_{eff} (μ_B)	$\Delta\delta$ (Hz)	χ_M^{para}	μ_{eff} (μ_B)	$\Delta\delta$ (Hz)	χ_M^{para}	μ_{eff} (μ_B)	$\Delta\delta$ (Hz)	χ_M^{para}	μ_{eff} (μ_B)
pa-HO[b]	275	18.97	3.94	2.63	32.25	6.70	3.43				27.21	5.67	3.15
	288	18.01	3.74	2.62	32.33	6.72	3.51				28.81	6.00	3.32
	298	17.37	3.61	2.62	32.33	6.72	3.57				31.29	6.48	3.51
	308	17.05	3.54	2.64	32.92	6.84	3.66				33.93	7.07	3.72
nm-HO[c]	275	16.81	3.94	2.63	28.73	6.73	3.43	73.54	17.23	5.49			
	288	16.08	3.77	2.63	29.21	6.84	3.54	70.26	16.46	5.49			
	298	15.52	3.64	2.63	31.13	7.29	3.72	67.78	15.88	5.49			
	308	15.05	3.53	2.63	34.01	7.97	3.95	66.02	15.47	5.51			

[a] $\chi_M^{para} \times 10^8$ is expressed in $m^3\ mol^{-1}$. [b] Paramagnetic and diamagnetic samples of *pa*-HO complexes were 1.8 mM. [c] Paramagnetic and diamagnetic samples of *nm*-HO complexes were 1.6 mM. [d] Data for resting state *pa*-HO are not included because this molecule exists as a mixture of high-spin (aqua) and low-spin (hydroxo) species at pH 7.0. At pH 6.7 and below, the *pa*-HO−heme complex is unstable. [e] The OH^- complex of *nm*-HO was not studied because the pK_a of the *nm*-HO−H_2O to *nm*-HO−OH transition is too high (9.3) to permit full formation of *nm*-HO−OH.

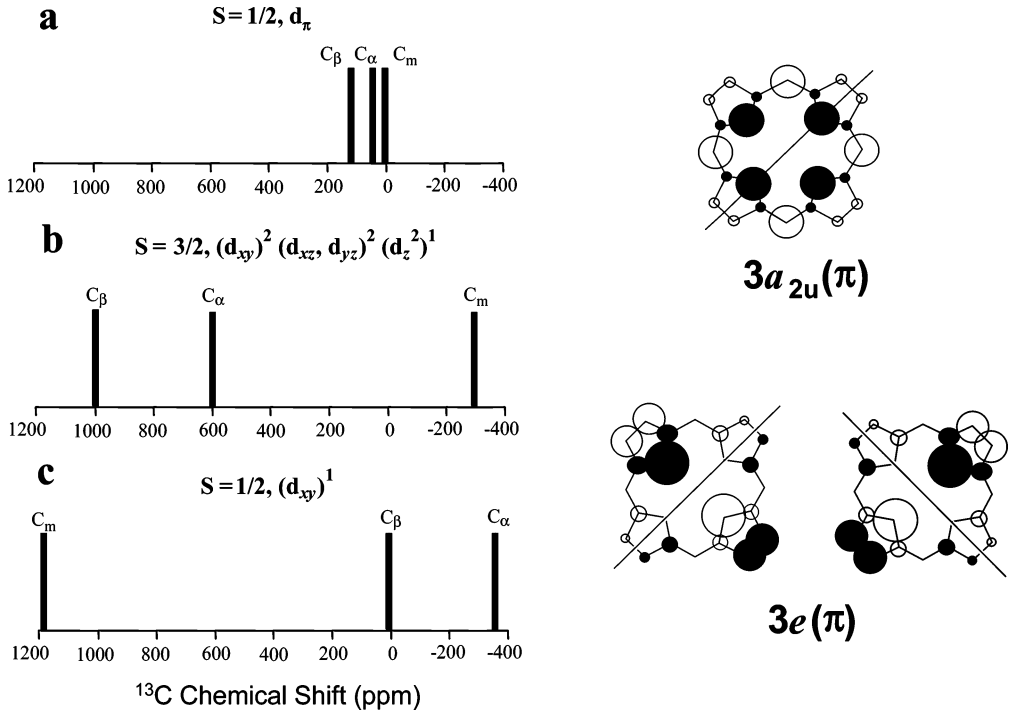

Figure 6. Left: Typical porphyrin core carbon chemical shifts corresponding to (a) Fe^{III}−porphyrinates with a d_π electron configuration; (b) Fe^{III}−porphyrinates with an $S = {}^3/_2$, d_π electron configuration; and (c) Fe^{III}−porphyrinates with an $S = {}^1/_2$, $(d_{xy})^1$ electron configuration. Right: Schematic representation of the $3a_{2u}(\pi)$ and $3e(\pi)$ porphyrin orbitals. The relative sizes of the circles at each atom are proportional to the calculated electron density.

Table 4. Correlation Table for the Molecular Orbitals of Metalloporphyrins[a,b]

	D_{4h}	D_{2h}	D_{2d}	C_{4v}
		metal		
$d_{x^2-y^2}$	b_{1g}	a_g	b_2 (b_1)	b_1
d_{z^2}	a_{1g}	a_g	a_1	a_1
d_{xz}, d_{yz}	e_g	b_{2g}, b_{3g}	e	e
d_{xy}	b_{2g}	b_{1g}	b_1 (b_2)	b_2
		porphyrin		
LUMO	e_g	b_{2g}, b_{3g}	e	e
HOMO	a_{1u}	a_u	b_1	a_2
	a_{2u}	b_{1u}	b_2	a_1
HOMO-1	e_g	b_{2g}, b_{3g}	e	e

[a] Symmetry representations for ruffled deformation are given in parentheses. [b] Table adapted from refs 68 and 69.

to *nm*-HO−CN (black) and to *nm*-HO−N_3 (red). At the lowest temperature, the downfield C_α and C_β shifts from the *nm*-HO−N_3 complex are significantly larger than those obtained from *nm*-HO−CN. The downfield C_α and C_β shifts of *nm*-HO−N_3 increase very rapidly with increasing temperature such that, at the higher temperatures, these shifts are much larger than the corresponding shifts from *nm*-HO−CN. In stark contrast, the average C_m shifts are essentially identical for both *nm*-HO−N_3 and *nm*-HO−CN at all temperatures. The magnitude and temperature dependence of the core carbon shifts observed with *nm*-HO−N_3 (Figure 8a) are very similar to those observed for the *pa*-HO−N_3 and *pa*-HO−OH complexes (Figure 8b,c, respectively), thus the following applies to the N_3^- complexes of *nm*-HO and *pa*-HO and the most abundant population of the OH^- complex of *pa*-HO. In the following discussion, the latter will be referred to simply as *pa*-HO−OH.

The unusual magnitude and steep temperature dependence of the C_α and C_β shifts and the almost diamagnetic position and temperature independence of the C_m shifts originating from *nm*-HO−N_3, *pa*-HO−N_3, and *pa*-HO−OH may be best explained by a dynamic equilibrium of two populations in rapid exchange relative to the NMR time scale. One population has the d_π electronic structure and planar heme, and the other exhibits an $S = {}^3/_2$, $(d_{xz},d_{yz})^3(d_{xy})^1(d_z^2)^1$ ($S = {}^3/_2$, d_{xy} hereafter)

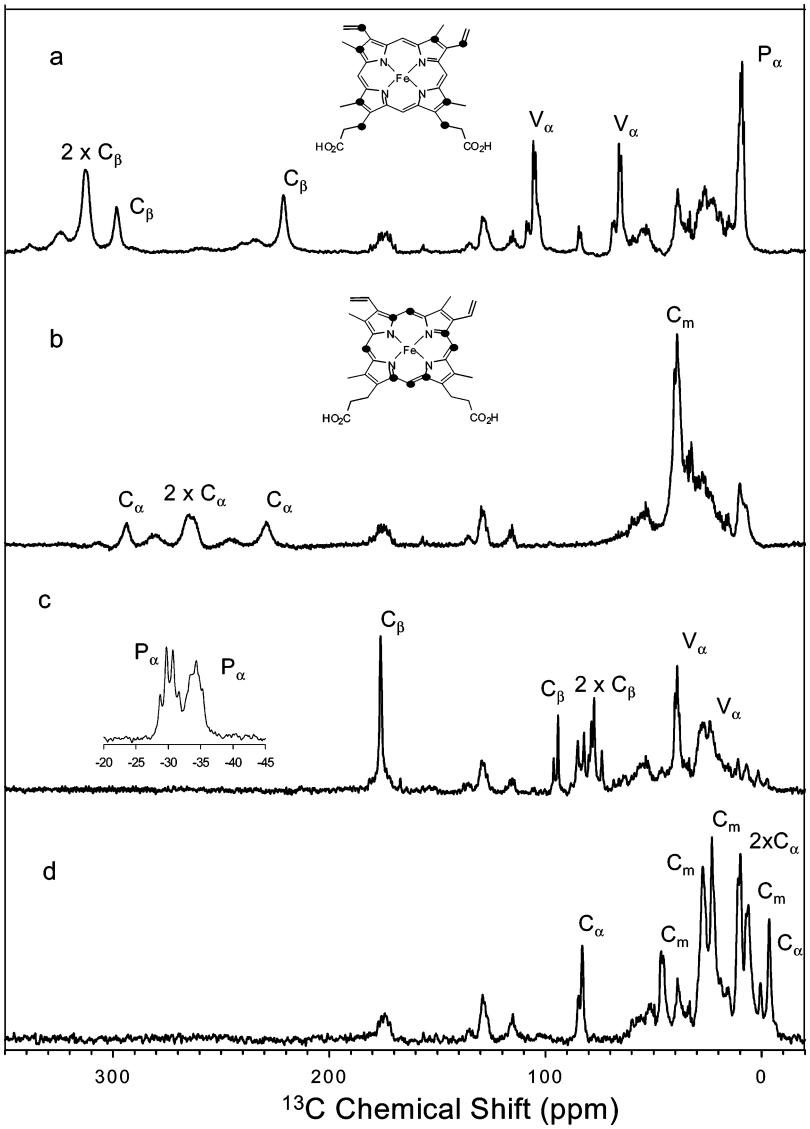

Figure 7. Nondecoupled ^{13}C NMR spectra (35 °C) of (a) *nm*-HO−N_3 reconstituted with heme labeled at carbons C_β, vinyl-α, and propionate-α; (b) *nm*-HO−N_3 reconstituted with heme labeled at carbons C_α and C_m. (c) and (d) *nm*-HO−CN reconstituted with heme labeled as in (a) and (b), respectively.

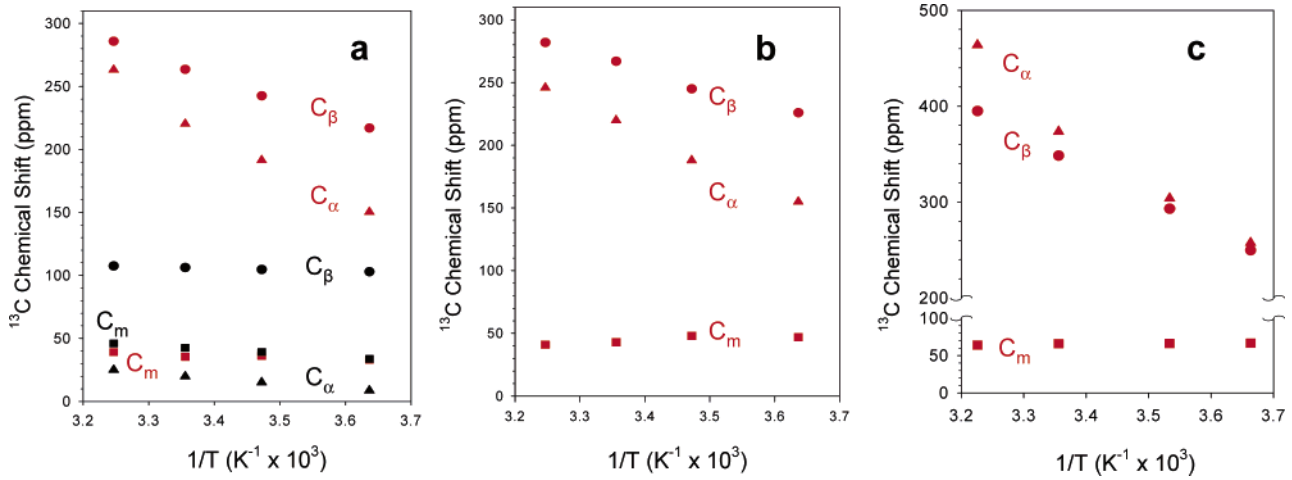

Figure 8. (a) Temperature dependence of core carbon chemical shifts corresponding to *nm*-HO−N_3 (red symbols) and *nm*-HO−CN (black symbols). Panels (b) and (c) show the temperature dependence of core carbon chemical shifts from *pa*-HO−N_3 and *pa*-HO−OH, respectively.

electron configuration and nonplanar macrocycle. In the population of molecules with the $S = {}^3/_2$, d_{xy} electron configuration, the unpaired electron residing in the d_{z^2} orbital does not have appropriate symmetry to interact with a planar hexacoordinated (D_{4h}) or with a nonplanar hexacoordinated heme (D_{2d}). Consequently, this unpaired electron is not expected to contribute

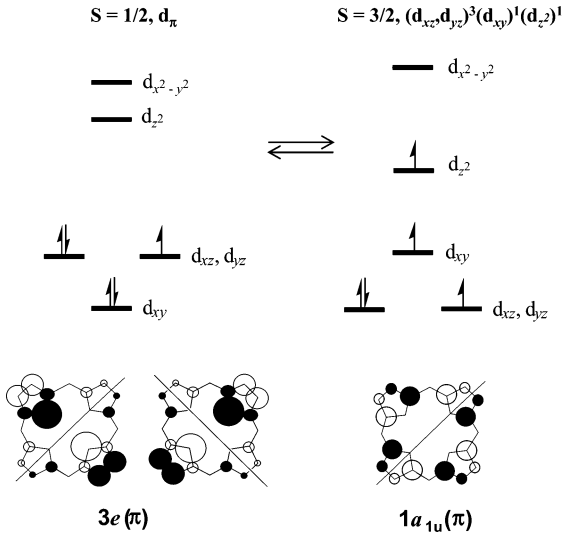

Figure 9. (Top) Schematic depiction of the equilibrium between d_π and $S = {}^3/_2$, d_{xy} electron configurations. (Bottom) Schematic representation of the 3e(π) and $1a_{1u}$ porphyrin orbitals.

to the porphyrin ^{1}H and ^{13}C shifts. In contrast, the iron d_π and porphyrin 3e(π) orbitals transform with the same representation in planar (e_g) as well as in nonplanar (e) hexacoordinated metalloporphyrins (see Table 4).[68] This implies that interactions between iron d_π and porphyrin 3e(π) orbitals are allowed by symmetry in planar and in nonplanar hexacoordinated hemes. Similar symmetry considerations indicate that the iron d_{xy} and porphyrin a_{1u} orbitals will be of the b_1 representation in nonplanar hexacoordinated hemes with D_{2d} symmetry (Table 4). This indicates that interactions between iron d_{xy} and porphyrin a_{1u} orbitals in nonplanar hemes are symmetry allowed, an observation that leads to the following explanation of the magnitude and temperature dependence of the core carbon chemical shifts from *nm*-HO−N_3 and *pa*-HO−N_3 and *pa*-HO−OH. Spin delocalization from the porphyrin 3e(π) orbitals into one of the iron d_π orbitals results in relatively large C_β shifts and somewhat smaller C_α shifts, as shown schematically in Figure 6a. In addition, spin delocalization from the porphyrin a_{1u} (shown schematically in Figure 9) to the iron d_{xy} orbital also contributes to the magnitude of the C_α and C_β shifts. Consequently, in ferrihemes with the $S = {}^3/_2$, d_{xy} electron configuration, symmetry allows simultaneous spin delocalization from C_α and C_β carbons into both, d_{xy} and d_π iron orbitals. This results in large spin density at the C_α and C_β positions and, therefore, larger C_α and C_β shifts relative to ferrihemes with the d_π electron configuration. This is in agreement with the magnitude of the C_α and C_β shifts obtained from *nm*-HO−N_3, *pa*-HO−N_3, and *pa*-HO−OH (Figure 8). The almost diamagnetic C_m shifts are also explained by an equilibrium between ferrihemes with d_π and $S = {}^3/_2$, d_{xy} spin states because the porphyrin 3e(π) and $a_{1u}(\pi)$ orbitals used for spin delocalization in both types of complexes have nodes through the meso carbons (see Figure 9).

The steep temperature dependence of the C_α and C_β shifts originating from the *nm*-HO−N_3, *pa*-HO−N_3, and *pa*-HO−OH complexes is also in agreement with an equilibrium between ferrihemes with the d_π and $S = {}^3/_2$, d_{xy} spin states. As the temperature increases, the population with the $S = {}^3/_2$, d_{xy} spin state and nonplanar heme grows and the effects of spin delocalization from the a_{1u} orbital become more dominant. This is manifested in the fact that the C_α shifts have steeper temperature dependence than the C_β shifts, as would be expected from the larger orbital coefficients (relative circle size) of the α-carbons in the schematic representation of the a_{1u} orbital. The shallow temperature dependence of the C_m shifts is consistent with the fact that the porphyrin 3e(π) and $a_{1u}(\pi)$ orbitals have nodes at the meso positions. Ferrihemes with a pure $S = {}^3/_2$, d_{xy} electron configuration are expected to have C_α shifts larger than C_β shifts. This is consistent with the trend exhibited by the C_α and C_β shifts (Figure 8a,b), which suggests that if it was possible to explore temperatures higher than ∼40 °C without denaturing the enzyme, the population of the $S = {}^3/_2$ species would increase further and the C_α shifts would become larger than the C_β shifts. It is evident from Figure 8c that this situation is attained in the most abundant population of the *pa*-HO−OH complex, which exhibits an average C_α shift greater than an average C_β shift at the higher temperatures. In a previous report, we indicated this population to be in an $S = {}^1/_2$, $S = {}^3/_2$ spin crossover.[32] Data obtained as part of this study show that the most abundant population of the *pa*-HO−OH complex, like the HO−N_3 complexes, exists as a mixture of ferriheme with a d_π electron configuration and planar macrocycle in equilibrium with ferriheme with an $S = {}^3/_2$, d_{xy} electron configuration and nonplanar heme. It is also noteworthy that the equilibrium between a population with a d_π electronic structure and planar heme and a population with an $S = {}^3/_2$, d_{xy} electronic structure and nonplanar heme, inferred from analysis of the ^{13}C data, is in agreement with the magnitude and temperature dependence of the μ_{eff} values obtained from *nm*-HO−N_3, *pa*-HO−N_3, and *pa*-HO−OH (Table 3).

Finally, it is interesting to point out that while this work was under review, a paper describing results from DFT calculations was published, indicating that bonding interactions between iron d_{xy} and porphyrin a_{1u} orbitals are indeed possible in saddled porphyrins.[69] Hence, our interpretation of the magnitude and temperature dependence of ^{13}C shifts originating from core heme carbons in the N_3^- and OH^- complexes of HO is supported by theoretical calculations. In the next section, we discuss the relevance of these observations to the chemistry of heme oxidation as performed by the enzyme heme oxygenase.

Mechanistic Implications for Heme Hydroxylation and Concluding Remarks

The results presented above indicate that binding of azide to the ferric resting state of *nm*-HO or *pa*-HO results in the formation of two populations in dynamic equilibrium; one attains a novel electronic configuration $S = {}^3/_2$, d_{xy} and nonplanar macrocycle, and the other exhibits the more common d_π electronic structure and planar heme. In this context, it is interesting to note that the electronic and conformational structure of the heme in HO is highly dependent on the nature of the sixth (distal) ligand. For example, when CN^- serves as the distal ligand in these enzymes, the corresponding NMR spectra are always indicative of planar hemes with a pure d_π electron configuration.[44,55,70−72] In contrast, when the distal

(68) Cheng, R.-J.; Chen, P.-Y.; Lovell, T.; Liu, T.; Noodleman, L.; Case, D. A. *J. Am. Chem. Soc.* **2003**, *125*, 6774−6783.

(69) Cheng, R.-J.; Wang, Y.-K.; Chen, P.-Y.; Han, Y.-P.; Chang, C.-C. *Chem. Commun.* **2005**, 1312−1314.

ligand is capable of accepting a hydrogen bond at the coordinating atom, such as OH^- [32] or N_3^- (this work), the resultant complex no longer exhibits the d_π electron configuration and planar heme typical of globins coordinated by these ligands.[39] Thus, when OH^- serves as the distal ligand, the heme in *pa*-HO adopts at least three populations, two of these, $(d_{xy})^1$ and $S = {}^3/_2$, d_π, place significant spin density at the meso positions,[32] and the third and most abundant exists in dynamic equilibrium between populations with the d_π and $S = {}^3/_2$, d_{xy} spin states. The *nm*-HO$-N_3$ and *pa*-HO$-N_3$ complexes also exist in equilibrium between two populations, one with the d_π electron configuration and planar heme and the second with an $S = {}^3/_2$, d_{xy} spin state and saddled heme.

On the basis of these observations, we propose that the coordinated OH^- or N_3^- ligand, by virtue of accepting a hydrogen bond to the coordinating atom, lower their σ-donating ability, thereby lowering their field strength. Decreasing axial ligand field strength is typically accompanied by (a) strengthening of the equatorial field, that is, shorter bonds between the iron and the pyrrole nitrogens, which induce nonplanar porphyrin deformations, and (b) stabilization of the d_z^2 orbital, which facilitates attainment of the $S = {}^3/_2$ electron configuration,[40,41] and/or stabilization of the d_π orbitals relative to the in-plane d_{xy} orbital, which is conducive to the $(d_{xy})^1$ electronic structure.[29,38,42,73] Consequently, if the field strength of the HOO^- ligand, which we surmise is similar to that of the OH^- ligand, is affected in a similar manner, the nonplanar deformations and large spin density at the meso carbons observed in the populations with the $(d_{xy})^1$ and $S = {}^3/_2$, d_π spin states would be expected to activate the heme (substrate) to actively participate in its own hydroxylation. For instance, when the distal ligand is OH^-, a small population attains the $(d_{xy})^1$ electron configuration, which places large spin density at the meso carbons due to partial porphyrin-to-metal electron transfer.[35,74,75] A limiting resonance structure for such species is that in which the electron is fully transferred from the porphyrinate ring to the metal and may be represented by **b** in Scheme 2. As was pointed out before, on the basis of studies with model complexes of the hydroperoxide intermediate in HO catalysis, this limiting resonance structure suggests the possibility of a radical mechanism for meso hydroxylation.[28] In this mechanism, attack of $^\bullet$OH at a meso carbon would produce **c**, which would arrange its Fe$-$O electron configuration, lose a proton from the attacked meso carbon to re-aromatize the porphyrin ring, and accept two protons to form the resting state complex **d**.

A radical mechanism was considered previously but not fully favored because attack of the $^\bullet$OH radical was thought to be too indiscriminate to account for the exquisite regioselectivity of heme hydroxylation characteristic of HO catalysis.[76] However, crystal structures[57,64] of HO coordinated by a distal O_2 or N_3^- strongly suggest that steric interactions between the distal ligand and residues in the distal helix not only orient the HOO^- moiety so that the terminal OH lies nearly on top of the α-meso carbon but also provide steric protection to the β-, γ-, and δ-meso carbons. Hence, electronic activation of the meso positions in response to the microenvironment of the HOO^- ligand, together with steric protection of all but one meso carbons, results in efficient and regioselective hydroxylation. Interestingly, a recent theoretical report suggested that heme hydroxylation by ferric hydroperoxo or oxoferryl species requires the surmounting of high energy barriers, 42.9 and 39.9 kcal/mol, respectively. This led the authors to suggest that there is an as yet "overlooked" factor that reduces the high activation barrier for heme hydroxylation.[77] A different theoretical study suggested that heme hydroxylation is more likely to occur by a homolytic cleavage of the O$-$O bond followed by trapping of the $^\bullet$OH radical by the heme in the form of meso hydroxyheme.[78] The notion derived from our experimental observations made with model complexes of the $Fe^{III}-OOH$ intermediate[28] and from studies conducted with HO coordinated by OH^- [32] or N_3^- as mimics of the HOO^- ligand suggests that the electronic structure of the $Fe^{III}-OOH$ complex in HO activates the heme to become an active participant in the hydroxylation reaction. Hence, it is likely that the electronic activation of the macrocycle in the $Fe^{III}-OOH$ complex is the overlooked factor that reduces the high barrier for heme hydroxylation. Further, if the hydroperoxide complex of HO behaves like the hydroxide complex, the significant spin density placed at the meso carbons in the populations with $(d_{xy})^1$ and $S = {}^3/_2$, d_π spin states is indeed consistent with a homolytic cleavage of the $Fe^{III}-OOH$ bond, followed by efficient trapping of the $^\bullet$OH radical by a sterically unprotected meso carbon bearing significant spin density. In this context, it is important to point out that the different populations with different electronic structures observed in the hydroxide complex of *pa*-HO are in dynamic exchange with one another.[32] This suggests that if the $Fe^{III}-OOH$ complex with $(d_{xy})^1$ and $S = {}^3/_2$, d_π spin states are reactive, the dynamic

Scheme 2

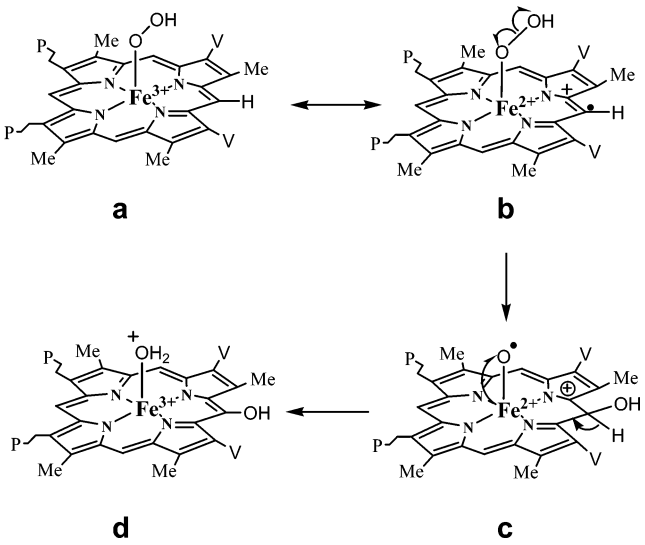

(70) Li, Y.; Syvitski, R. T.; Auclair, K.; Ortiz de Montellano, P. R.; La Mar, G. N. *J. Am. Chem. Soc.* **2003**, *125*, 13392−13403.
(71) Hernandez, G.; Wilks, A.; Paolesse, R.; Smith, K. M.; Ortiz de Montellano, P. R.; La Mar, G. N. *Biochemistry* **1994**, *33*, 6631−6641.
(72) Li, Y.; Syvitski, R. T.; Chu, G. C.; Ikeda-Saito, M.; La Mar, G. N. *J. Biol. Chem.* **2003**, *278*, 6651−6663.
(73) La Mar, G. N.; Bold, T. J.; Satterlee, J. D. *Biochim. Biophys. Acta* **1977**, *498*, 189−207.
(74) Walker, F. A.; Nasri, H.; Torowska-Tyrk, I.; Mohanrao, K.; Watson, C. T.; Shkhirev, N. V.; Debrunner, P. G.; Scheidt, W. R. *J. Am. Chem. Soc.* **1996**, *118*, 12109−12118.
(75) Simonneaux, G.; Schünemann, V.; Morice, C.; Carel, L.; Toupet, L.; Winkler, H.; Trautwein, A. X.; Walker, F. A. *J. Am. Chem. Soc.* **2000**, *122*, 4366−4377.
(76) Wilks, A.; Torpey, J.; Ortiz de Montellano, P. R. *J. Biol. Chem.* **1994**, *269*, 29553−29556.
(77) Kamachi, T.; Shestakov, A. F.; Yoshizawa, K. *J. Am. Chem. Soc.* **2004**, *126*, 3672−3673.
(78) Sharma, P. K.; Kevorkiants, R.; de Visser, S. P.; Kumar, D.; Shaik, S. *Angew. Chem., Int. Ed.* **2004**, *43*, 1129−1132.

Scheme 3

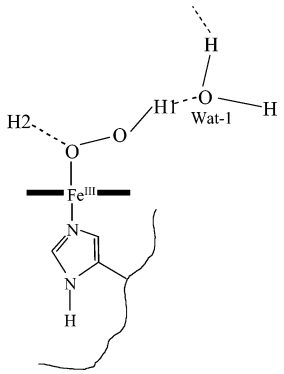

equilibrium relating the different spin states continuously replenishes the reactive form. In other words, dynamic exchange allows complete conversion of $Fe^{III}-OOH$ into meso hydroxyheme despite the low equilibrium concentrations of the reactive species.

On the basis of these findings and in the context of advances made by several other investigators, a set of events conducive to heme hydroxylation can perhaps be summarized as follows. Injection of a second electron to the oxyferrous complex results in the formation of a nascent $Fe^{III}-OO^-$ complex, which is readily protonated (H1 in Scheme 3) by a structured water molecule, which subsequently acts as a hydrogen bond acceptor to the $Fe^{III}-OOH$ moiety, thereby slowing down the rate of cleavage of the O−O bond.[26,79,80] ENDOR studies demonstrated that in the reactive form of the $Fe^{III}-OOH$ complex, obtained only after annealing the $Fe^{III}-OOH$ intermediate above 200 K, a second well-defined ^1H signal (H2 in Scheme 3) is observed.[26] We suggest that H2 donates a hydrogen bond to the coordinated oxygen atom of the $Fe^{III}-OOH$ moiety, thus decreasing its σ-donating and field strength. The reduced field strength of the coordinated HOO^- ligand would be expected to induce the electronic structures and nonplanar distortions that place significant spin density at the heme meso positions. Hence, electronic activation of the substrate (heme) not only lowers the barrier for heme hydroxylation but also facilitates perhaps a radical mechanism for this reaction.

Acknowledgment. This work was supported by NIH Grants GM-50503 (M.R.) and AI-48551 (A.W.).

Supporting Information Available: Figure S1, ^1H NMR spectra of *pa*-HO titrated with sodium azide. Figure S2, WEFT-NOESY spectrum of azide-inhibited *pa*-HO. Figure S3, temperature-dependent ^1H NMR spectra of *pa*-HO−N_3, *pa*-HO−OH, and *nm*-HO−N_3. Figure S4, nondecoupled ^{13}C NMR spectra of azide-inhibited *pa*-HO. This material is available free of charge via the Internet at http://pubs.acs.org.

JA0425987

(79) Lad, L.; Wang, J.; Li, H.; Friedman, J.; Bhaskar, B.; Ortiz de Montellano, P. R.; Poulos, T. L. *J. Mol. Biol.* **2003**, *330*, 527−538.
(80) Fujii, H.; Zhang, X.; Tomita, T.; Ikeda-Saito, M.; Yoshida, T. *J. Am. Chem. Soc.* **2001**, *123*, 6475−6484.